The model of nuclear structure

Michael Tzoumpas
Mechanical and Electrical Engineer
National Technical University of Athens
Irinis 2, 15234 Athens, Greece

E-mail: m.tzoumpas@gmail.com

May 2024

Abstract. The structure of nuclei begins with lower-order nuclei, such as deuterium, tritium, and helium $He-3$, which evolve into the helium nucleus $He-4$, and then the first upper-order oxygen nucleus $O-16$ that has four helium nuclei $He-4$ in a column of strong negative electric field. Furthermore, the second upper-order calcium nucleus Ca is based on the fundamental natural phenomenon of mirror symmetry, by repeating the structure of the first upper-order oxygen nucleus and its half, i.e., at a 2.5 factor. The same principle applies to the third upper-order tin nucleus Sn, which emerges from the second upper-order calcium nucleus Ca, according to mirror symmetry and the same 2.5 factor. It is noted that the tin nucleus Sn will further form the basis for the structure of all heavy nuclei up to the radioactive uranium nucleus $U-235$. This is the simple and elegant structure model, according to which nuclei consist of fixed helium nuclei $He-4$ (plus deuterium, tritium, and helium $He-3$, all evolving into helium $He-4$), while the bonding neutrons rotate around them.

Keywords: Lower and upper-order nuclei; bonding neutrons; mirror symmetry.

PACS numbers: 12.60.-i

1. Introduction

The Unified Theory of Dynamic Space,[1] conceived and written by Professor Physicist Naoum Gosdas, is inspired by the principle of antithesis (opposition), which is believed to be the driving force behind the creation of all natural phenomena. According to this theory, these phenomena are derived from a unique absolute dynamic space, structured with fundamental elements: dimension, elementary electric charges (units), and the forces that create the universal cohesive pressure,[2] denoted as P_0.

According to this theory, nuclei[3] are structured through two fundamental phenomena: the inverse electric field of the proton and the electric entity of the neutron.

1.1. The inverse electric and nuclear field

The positive charge of a proton causes the electrical induction of positive and negative units,[1,4] creating electric or quantitative deformation of the proximal space, consisting of the repulsion of positive units and the attraction of negative ones. This results in the alteration of the background electric density, ρ_0, which is the density of electric charge per length (Cb/m) of an equal number of positive and negative units. We define $\rho(+)$ and $\rho(-)$ as the equal relative densities of positive or negative units per length, respectively. Thus, the absolute value of the electric density is given by

$$\rho_a = \rho_0 + \rho(+) \Rightarrow \rho_a = \rho_0 + \rho(-). \tag{1}$$

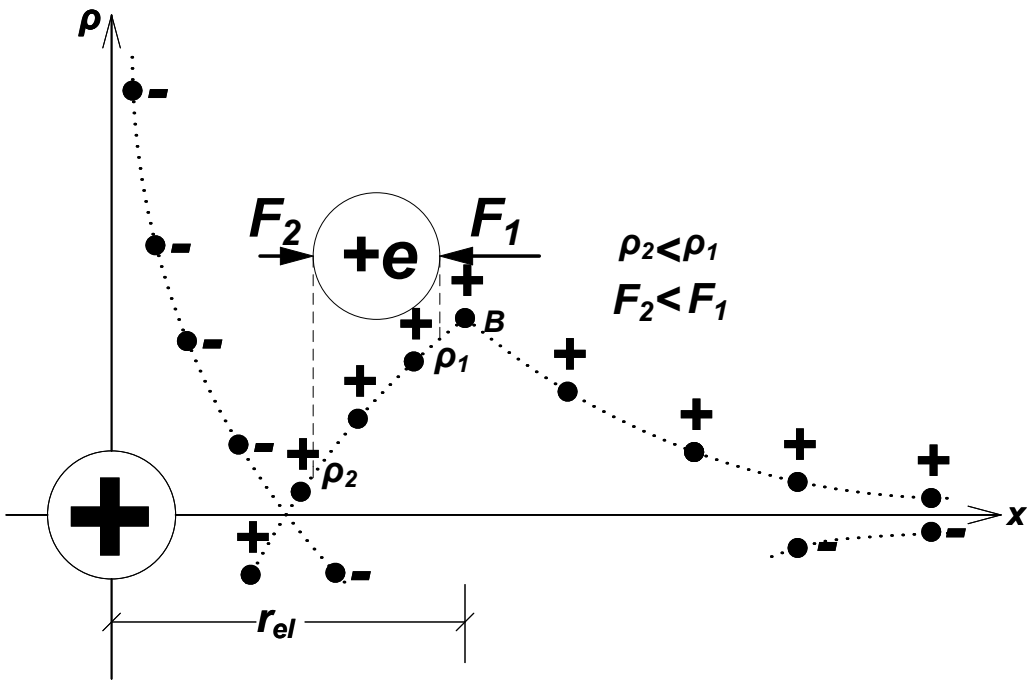

Figure 1. Attraction of a proton at the nuclear field, where B is the potential barrier ($F_1 = Ke\rho_1$, $F_2 = Ke\rho_2$, $\rho_2 < \rho_1$; hence $F_2 < F_1$), and r_{el} is the nucleus's electric radius[3]

The proton (indicated in Fig. 1) with electric charge $+e$ is at position $x = 0$, where the background electric density ρ_0 of the positive and negative units was, while the axes represent the relative electric density ρ (proportional to the potential V of the electric field) and the distance x, i.e.,

$$\rho = \frac{e}{x}. \tag{2}$$

The top of the hill is the potential barrier B, within which the inverse (inner) electric field extends, and externally the outer electric field extends, whose electric intensity declines until the distance x.

In the outer electric field of a proton, which extends beyond the potential barrier, the positive units outnumber the background electric density, while the reduction of the

negative ones is also equal. Consequently, a positive charge is repelled from the proton due to the higher electric density of units on the proton side.

In the inverse electric field (to the left of B), a positive charge is attracted by the proton, repelled more strongly by the units of higher electric density on the right of the positive charge, but less strongly by the units of lower electric density on the left of the positive charge (see Fig. 1, $\rho_2 < \rho_1$ hence $F_2 < F_1$). Therefore, in the inverse electric field, the "paradox" occurs where a positive charge is attracted by the positive proton. This is the opposite of what happens in the outer electric field, resulting in like charges being attracted and oppositely charged particles being repelled. This phenomenon is confirmed by the braking radiation emitted from rapidly moving electrons as they pass close to the nucleus and are not attracted to them but repelled due to the inverse electric field, thereby slowing down by radiating.

Thus, we conclude that protons in the nucleus, due to the inverse electric-nuclear field, are not repelled but attracted. Therefore, the strong nuclear force is the electric-nuclear force of the inverse electric field.

1.2. Electric entity of the neutron

The surface electric charge q_n of the neutron[5] can be calculated from its magnetic dipole moment $\mu = -1.913\mu_n$ and the magnetic dipole moment of the proton $\mu' = +2.792\mu_n$, where its electric charge is $e = +1.6 \times 10^{-19}$ C.

These magnetic moments μ and μ' must be proportional to the electric charges q_n (neutron) and e (proton), respectively, such that

$$\frac{q_n}{e} = \frac{\mu}{\mu'} = \frac{-1.913\mu_n}{2.792\mu_n} \Rightarrow q_n = -0.685e, \tag{3}$$

which equals the electric charge of the two negative poles (d quarks) of the neutron cortex[3] (Fig.2). Thus, the neutron consists of two d quarks (each with a $-e/3$ negative surface charge) and one intermediate u quark ($+2e/3$). Therefore, the total charge of the neutron is

$$-\frac{e}{3} + \frac{2e}{3} - \frac{e}{3} = 0. \tag{4}$$

Thus, macroscopically, the neutron is an electrically neutral particle. At the scale of nuclei, however, the neutron behaves as a positively charged particle because the above negative surface charge $q_n = -0.685e$ creates an inverse electric field of positive potential, forming a cloud of positive electric units (Fig.2). Upon entering the nuclear field (indicatively see Fig. 3), it affects its negativity (as well as the cohesive pressure, see subsection 1.5) and contributes to the architectural structure of the nuclei.

It is noted that two protons cannot exist in the nucleus without the presence of a neutron, as the increased negativity of the field causes one proton to undergo cleavage (beta decay β^+). Nuclei would not exist without the presence of neutrons, which reduce the negativity of the proton's field.

1.3. Magnetic moments of nuclei

The magnetic dipole moment of the nucleus is the sum of the magnetic moments of the nucleons or of the lower- and upper-order nuclei and of the additional bonding neutrons. The lower-order nuclei include deuterium ${}^{2}_{1}H$, tritium ${}^{3}_{1}H$, helium ${}^{3}_{2}He$, and helium ${}^{4}_{2}He$, with corresponding experimental magnetic moments of $\mu = 0.857\mu_n$, $\mu = 2.978\mu_n$, $\mu = 2.127\mu_n$, and $\mu = 0$, where μ_n is the unit of nuclear magneton. Additionally, $\mu = 2.792\mu_n$ is the magnetic moment of the proton, and $\mu = -1.913\mu_n$ is the magnetic moment of the neutron.

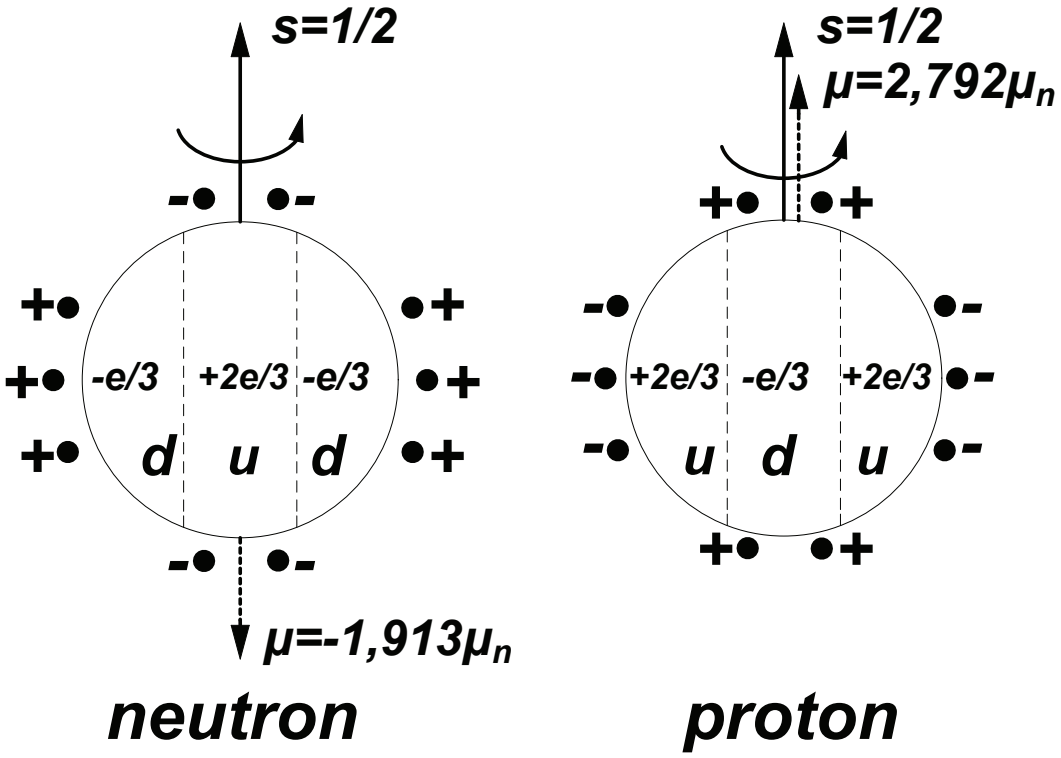

Figure 2. Spin and magnetic dipole moment of the neutron and proton with their respective lower inverse electric fields

Also, the experimental magnetic moment of helium ${}^{4}_{2}He$ and the three upper-order nuclei (oxygen, calcium, and tin), as well as those constructed from them, have a magnetic moment of $\mu = 0$. It is expected that the magnetic moments of nucleons align along a common axis and interact with each other. Additionally, it is noted that during the interaction of a proton and a neutron, the magnetic moment of these nucleons is increased, while during the interaction of identical nucleons, their magnetic moment is reduced.[3]

1.4. The fluctuation of nucleons magnetic moment

The inductive-inertial phenomenon[3] is observed during the spin of particles, wherein the quarks act as moving electric charges. Thus, the +2e/3 quarks (two positive poles) of

the proton spin easily emit negative grouping units[5] in front. These units are abundant in the inverse electric field of the proton (Figs 1 and 2), which has difficulty repelling positive grouping units behind due to their scarcity. As a result, the proton's magnetic moment is reduced, which is attributed to these alternate electric charges.

Similarly, the -e/3 quarks (two negative poles) of the neutron spin easily emit positive grouping units in front. These units are abundant in the inverse electric field of the neutron (Fig. 2), which has difficulty repelling negative grouping units behind due to their scarcity. As a result, the neutron's magnetic moment is reduced, which is due to these alternate electric charges.

However, this situation improves significantly in the nuclear environment. As the rotating neutron enters the lower inverse nuclear field (indicatively see Fig. 3), which has negative units in abundance, it acquires the possibility to increase the grouping units of quarks by sending negative units behind and positive ones in front, thereby increasing the magnetic dipole moment of the neutron. Additionally, with the entrance of the neutron and its positive units into its lower field, the proton's electric field is enhanced. Therefore, the proton is facilitated in repulsing the positive units behind and an equal number of negative ones in front, thereby increasing its magnetic dipole moment.

In contrast, during the interaction of identical nucleons, their magnetic dipole moment is reduced.

1.5. The spin and mass defect indicate the topology of nuclei

Verification of the experimental spin of the nuclei, due to the conservation of their rotational momentum, is the first and necessary condition for understanding their structure. The nucleons' spin is the sum of their individual spins and is directed parallel to the nucleus axis, while their orbits are perpendicular to this axis. Therefore, spin indicates the topology of the nucleons and the lower-order nuclear units within the nucleus.

In the inverse electric field of the nucleus (Fig. 1) the change in its relative electric density ρ directly affects the cohesive pressure of the proximal space, as it depends on the number of pairs of electrically opposite elementary units that remain in the electric field and cause tensions between these electric units.

Specifically, the remaining cohesive pressure P is proportional to these pairs of electrically opposite units, which remain in the electric field, especially in the lower one, where this change happens rapidly. So, if ρ is the relative electric density at a position in the inverse electric field, then the absolute electric density $\rho_0 - \rho$ is proportional to the number of the above pairs of units, whose attractive forces create the remaining cohesive pressure P at this position. Consequently, the cohesive pressures P_0 and P are respectively proportional to the background electric density ρ_0 and the absolute one $\rho_0 - \rho$, that is

$$\frac{P}{P_0} = \frac{\rho_0 - \rho}{\rho_0} \Rightarrow P = P_0 \frac{\rho_0 - \rho}{\rho_0}. \tag{5}$$

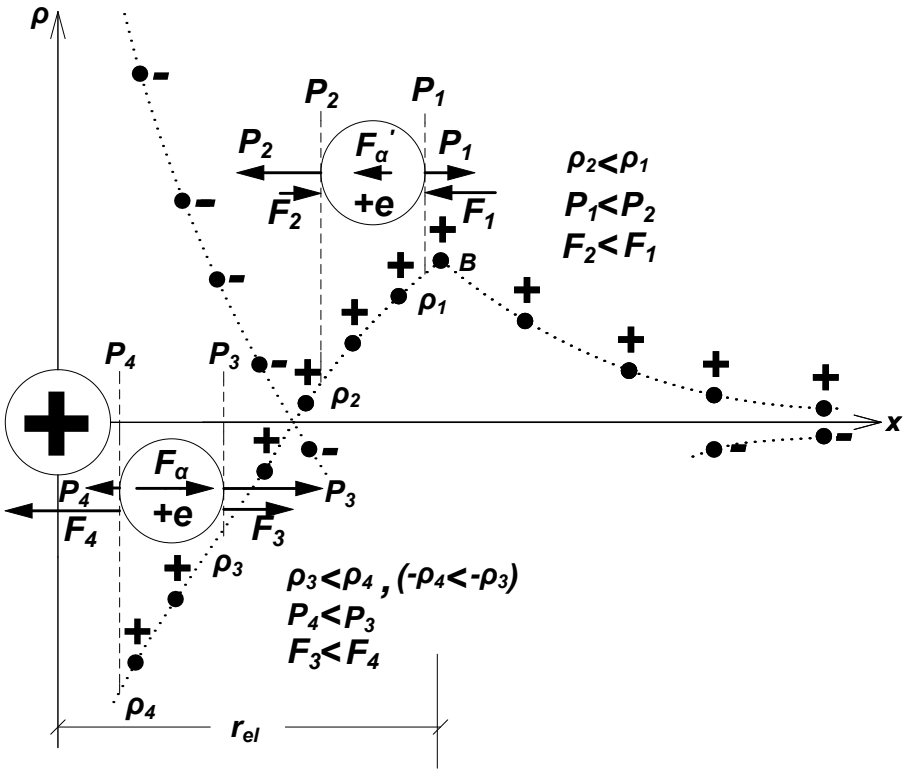

Figure 3. In the upper inverse nuclear field, the antigravity force F_a' and the electric resultant $F_1 - F_2$ are attractive, while in the lower field, a strong repulsive antigravity force[5] F_a balances the attractive electric resultant $F_4 - F_3$, i.e., the strong nuclear force

The cohesive pressure P_0 at the core vacuum[4] of a neutron (of radius r) causes a gravitational force, as shown in Eq. 6

$$F_0 = 4\pi r^2 P_0 \tag{6}$$

where the dynamic energy is given by

$$E_0 = F_0 L_0 = P_0 V. \tag{7}$$

Here, L_0 is the quantum dipole length,[5] i.e., the distance between two units, and

$$V = 4\pi r^3 \tag{8}$$

represents the volume of the neutron's core vacuum. Thus, the gravitational mass is

$$m_0 = \frac{E_0}{c^2} = \frac{F_0 L_0}{c^2} \Rightarrow m_0 = \frac{F_0 L_0}{c^2}. \tag{9}$$

The dynamic energy of a neutron, due to Eqs 6 and 8, becomes

$$E_0 = F_0 L_0 = P_0 V = \frac{P_0 4\pi r^3}{3} = \frac{(P_0 4\pi r^2) r}{3} = \frac{F_0 r}{3} \Rightarrow E_0 = \frac{F_0 r}{3}. \tag{10}$$

This decreases proportionally to F_0 and r. Therefore, the reduction of cohesive pressure (Eq. 5) in the lower inverse electric field creates a reduction of the gravitational force

F_0 (Eq. 6) and the dynamic energy of the neutron (Eq. 10), resulting in a shrinkage of its core's vacuum and its mass defect Δm (Eq. 9), which makes the neutron stable in this field.

However, for the protons, there is no mass defect. When a proton enters the lower inverse nuclear field, the cohesive pressure P_0 of the field decreases further (Fig. 3), due to the increase in negative units of the above nuclear field. This negativity in the environment of the lower field causes an attractive force on the positive cortex of the proton, balancing its potential shrinkage and loss of energy-mass. Therefore, the role of protons is to create the inverse electric field, while neutrons suffer the consequences of the mass defect. However, protons contribute to the increase in the nucleus's mass deficit because they increase (by entering the nuclear field) the negativity of the field, thus contributing to the reduction of cohesive pressure P_0 and therefore to the increase in the neutrons' mass defect.

Neutrons incur a mass defect only, while protons contribute to its creation. The mass defect depends solely on the negativity of the nuclear field. Therefore, the mass defect also determines the topology of nucleons and nuclear units in the nucleus.

Additionally, a proton entering the nucleus can be cleaved (beta decay β^+) at the strong negative potential of the field, which is reduced by the entering of the neutron into the nucleus. Conversely, a greater reduction in the negativity of the nuclear field may cause neutron cleavage (beta decay β^-) and a reduction in mass deficit due to increased cohesive pressure. Specifically, the locations of these phenomena in the nucleus are determined by beta decay β^- and β^+.

As we mentioned, at the nucleus scale, the neutron behaves as a positively charged particle and repels the closest proton, which now moves on a helical orbit emitting gamma radiation and is finally immobilized due to the balance between the attractive electric-nuclear force and the strong repulsive antigravity force.‡ This radiant energy of the proton, transmitted by the neutron, is measured as mass defect Δm and is equal to half of the kinetic energy of the neutron. Therefore, neutrons are the ones that move into the nuclei (with the remaining half of their kinetic energy) on circular orbits around immobilized protons, which only have spin. If protons were rotating, they would cause orbital magnetism, which has never been observed, beyond the magnetic dipole moment of nucleon spin. In addition, no regression of protons has occurred, because it would cause alternating magnetism, which has not been observed.

It is noted that attraction is exerted by the proton's electric field only, causing the neutron to sink deeper into its lower inverse field. After all, there are nuclei whose neutrons are rotated around columns of strong electric fields, known as the so-called bonding neutrons (see Fig. 9), in addition to those that rotate around the protons.

‡ In the lower inverse nuclear field, where the relative electric densities are $-\rho_4 < -\rho_3$ (or $\rho_3 < \rho_4$) and for $\rho = \rho_3$, $\rho = \rho_4$ the respective cohesive pressures P_3 and P_4 are $P_3 = P_0(\rho_0 - \rho_3)/\rho_0$, $P_4 = P_0(\rho_0 - \rho_4)/\rho_0$ (Eq. 5). Thus, $P_4 < P_3$, and $\Delta P = P_3 - P_4$. The buoyancy conditions create a repulsive antigravity force[5] $F_a = V\Delta P/\Delta x$ on the core's vacuum of proton (Fig. 3), balancing the attractive electric resultant $F_4 - F_3$ (nuclear force).

2. The Structure of Lower-Order Nuclei

2.1. Structure model of deuterium nucleus ${}^2_1H$

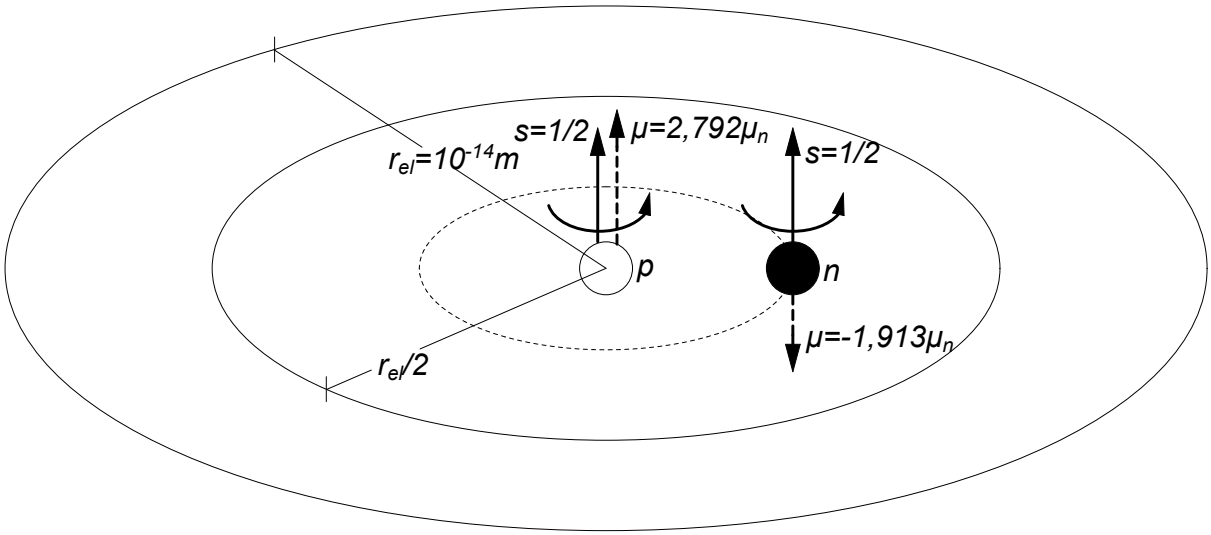

Figure 4. Structure model of the deuterium nucleus ${}^2_1H = p + n$, with an experimental spin of $s = 1/2 + 1/2 = 1$ and an experimental magnetic moment of $\mu = (2.792 + a)\mu_n - (1.913 + a + 0.022)\mu_n = 0.857\mu_n$, where $a\mu_n$ represents the increase in the magnetic moment of the proton (p) and $(a + 0.022)\mu_n$ represents the increase in the magnetic moment of the neutron (n). Here, $rel \approx 10^{-14}$m is the electric radius (Fig. 1) of the nucleus, and $r_{el}/2$ is the allowed orbit radius of the neutron. The small mass defect of deuterium, $\Delta m = 2.2$MeV, is identical to that of the neutron. This indicates that the neutron is not deeply embedded in the nuclear field

The deuterium nucleus

$$ {}^2_1H = {}^1_1 H + n = p + n \Rightarrow {}^2_1 H = p + n \tag{11}$$

is derived from hydrogen nucleus ${}^1_1H$ by addition of one neutron and has an experimental spin

$$ s = \frac{1}{2} + \frac{1}{2} = 1 \Rightarrow s = 1 \tag{12}$$

and an experimental magnetic dipole moment

$$ \mu = (2,792+a)\mu_n - (1,913+a+0,022)\mu_n = 0,857\mu_n \Rightarrow \mu = 0,857\mu_n, \tag{13}$$

where

$$ \mu' = a\mu_n \tag{14}$$

is the increase magnetic moment of proton and

$$ \mu'' = (a + 0,022)\mu_n \tag{15}$$

is the increase magnetic moment of neutron (see subsection 1.4).

The experimental mass defect of deuterium nucleus

$$\Delta m = 2,2MeV \tag{16}$$

is identical to that of neutron, which is stable now.

The electric radius of deuterium nucleus is[3] (Figs 1 and 3)

$$r_{el} \approx 10^{-14}m, \tag{17}$$

while $r_{el}/2$ is the allowed orbit radius of neutron.

2.2. Structure model of tritium nucleus ${}^3_1H$

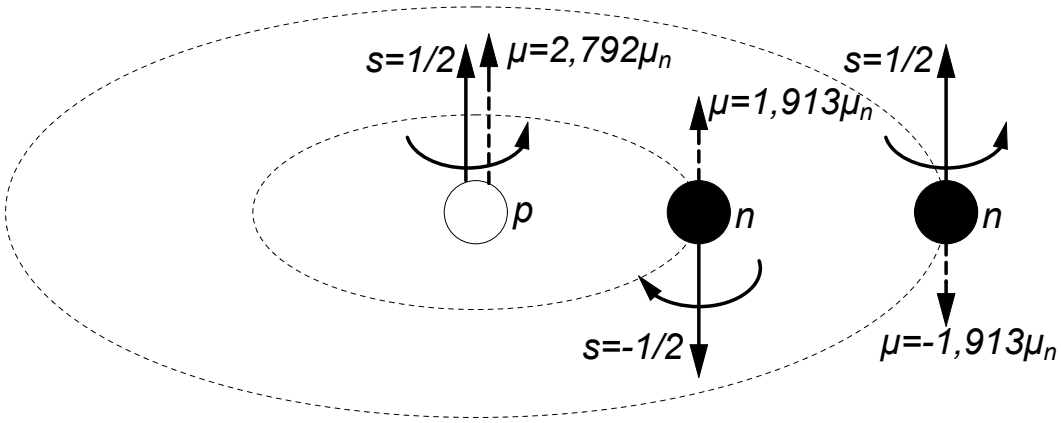

Figure 5. Structure model of the tritium nucleus ${}^3_1H = p+n+n$, with an experimental spin of $s = 1/2 - 1/2 + 1/2 = 1/2$ and an experimental magnetic moment of $\mu = (2.792 + 0.186 - c)\mu_n + (1.913 + b)\mu_n - (1.913 + b - c)\mu_n = 2.978\mu_n$. Here, $(0.186 - c)\mu_n$ represents the increase in the magnetic moment of the proton, $b\mu_n$ represents that of the nearest neutron, and $(b - c)\mu_n$ represents that of the distant neutron. The mass defect of tritium is $\Delta m = (4.24+d)+(4.24-d) = 8.48$MeV, where $(4.24 + d)$MeV is the mass defect of the nearest neutron and $(4.24 - d)$MeV is that of the distant neutron

The tritium nucleus

$${}^3_1H = p + n + n \tag{18}$$

is derived from deuterium nucleus (Fig. 4) by addition of one neutron (with opposite magnetic moment) between the proton and the initial neutron and has an experimental spin

$$s = \frac{1}{2} - \frac{1}{2} + \frac{1}{2} = \frac{1}{2} \Rightarrow s = \frac{1}{2} \tag{19}$$

and an experimental magnetic dipole moment

$$\mu = (2,792+0,186-c)\mu_n+(1,913+b)\mu_n-(1,913+b-c)\mu_n = 2,978\mu_n, \tag{20}$$

where

$$\mu' = (0,186 - c)\mu_n \tag{21}$$

is the increase magnetic moment of proton,

$$\mu'' = b\mu_n \tag{22}$$

is the increase magnetic moment of the nearest neutron and

$$\mu''' = (b - c)\mu_n \tag{23}$$

is the increase magnetic moment of the distant neutron.

The experimental mass defect of tritium nucleus (due to the two neutrons) is

$$\Delta m = (4,24 + d) + (4,24 - d) = 8,48MeV \Rightarrow \Delta m = 8,48MeV, \tag{24}$$

where

$$\Delta m' = (4,24 + d)MeV \tag{25}$$

is the mass defect of the nearest neutron and

$$\Delta m'' = (4,24 - d)MeV \tag{26}$$

is the mass defect of the distant neutron.

As the second neutron enters the deuterium nucleus, between the proton and the neutron, the negativity of the field decreases, causing the initial neutron to move to a more distant orbit and reducing its mass defect, making this neutron unstable. Therefore, tritium is an unstable nucleus.

2.3. Structure model of helium nucleus ^3_2He

The helium nucleus ^3_2He has the same mass number (A = 3) with the tritium, whose the unstable neutron cleaves (beta decay β^-)

$$n = p + e^- + \bar{\nu} \tag{27}$$

and the resulting proton accelerated in the inverse field and finally balanced, due to the strong repulsive antigravity force,§ radiating all its kinetic energy.

So, the helium nucleus ^3_2He (Fig. 6)

$$^3_2He = p + p + n \tag{28}$$

has an experimental spin

$$s = -\frac{1}{2} + \frac{1}{2} + \frac{1}{2} = \frac{1}{2} \Rightarrow s = \frac{1}{2} \tag{29}$$

and an experimental magnetic dipole moment

$$\mu = (-2,792 + 2,792)\mu_n - (1,913 + 0,214)\mu_n = -2,127\mu_n, \tag{30}$$

§ In the lower inverse nuclear field, where the relative electric densities are $-\rho_4 < -\rho_3$ (or $\rho_3 < \rho_4$) and for $\rho = \rho_3$, $\rho = \rho_4$ the respective cohesive pressures P_3 and P_4 are $P_3 = P_0(\rho_0 - \rho_3)/\rho_0$, $P_4 = P_0(\rho_0 - \rho_4)/\rho_0$ (Eq. 5), so $P_4 < P_3$ and $\Delta P = P_3 - P_4$. So, the buoyancy conditions creates a repulsive antigravity force[5] $F_a = V\Delta P/\Delta x$ on the core's vacuum of proton (Fig. 3), that balances the attractive electric resultant $F_4 - F_3$ (nuclear force).

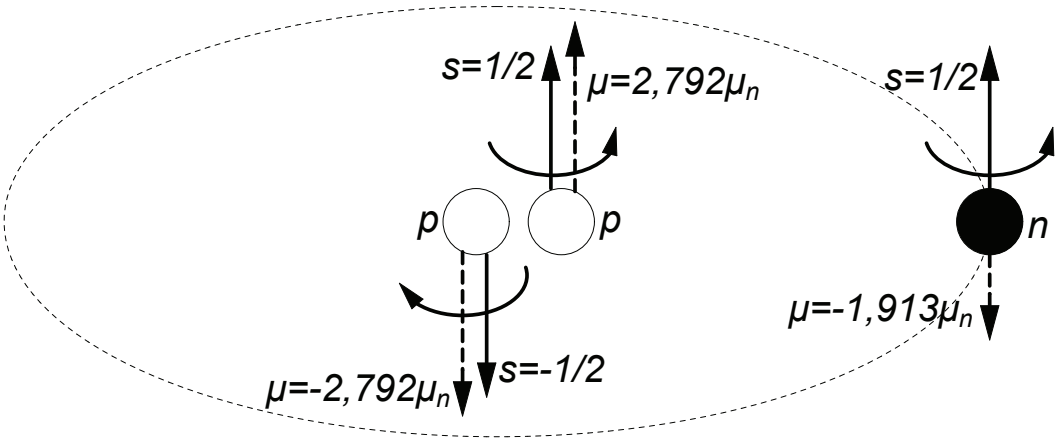

Figure 6. Structure model of helium nucleus ${}^3_2He = p + p + n$, with experimental spin $s = -1/2 + 1/2 + 1/2 = 1/2$ and with experimental magnetic moment $\mu = (-2,792+2,792)\mu_n-(1,913+0,214)\mu_n = -2,127\mu_n$. The mass defect of helium ${}^3_2He$ ($\Delta m = 7,69$MeV) is for the neutron only

where

$$\mu' = (-2,792 + 2,792)\mu_n = 0 \Rightarrow \mu' = 0 \tag{31}$$

is the sum magnetic moments of the two protons and

$$\mu'' = (1,913 + 0214)\mu_n \tag{32}$$

is the increase magnetic moment of neutron.

The increased mass defect (experimental) of helium nucleus ${}^3_2He$ is

$$\Delta m = 7,69MeV, \tag{33}$$

that is the value of the neutron.

2.4. Structure model of helium nucleus ${}^4_2He$

The two protons of the helium nucleus ${}^4_2He$ are very close due to the balance between the two strong forces: the nuclear force and the antigravity force. They have opposite spins and magnetic moments, creating a strong negative field that would instantly cause them to cleave (beta decay β^+). However, the presence of the two neutrons in the inverse electric field reduces its negativity and prevents this decay, making the helium nucleus ${}^4_2He$ the most stable nucleus in nature.

So, the helium nucleus ${}^4_2He$ (Fig. 7)

$${}^4_2He = n + p + p + n \tag{34}$$

has an experimental spin

$$s = -\frac{1}{2} - \frac{1}{2} + \frac{1}{2} + \frac{1}{2} = 0 \Rightarrow s = 0 \tag{35}$$

and an experimental magnetic dipole moment

$$\mu = (1,913+f)\mu_n-(2,792+g)\mu_n+(2,792+g)\mu_n-(1,913+f)\mu_n = 0, \tag{36}$$

so

$$\mu = 0. \tag{37}$$

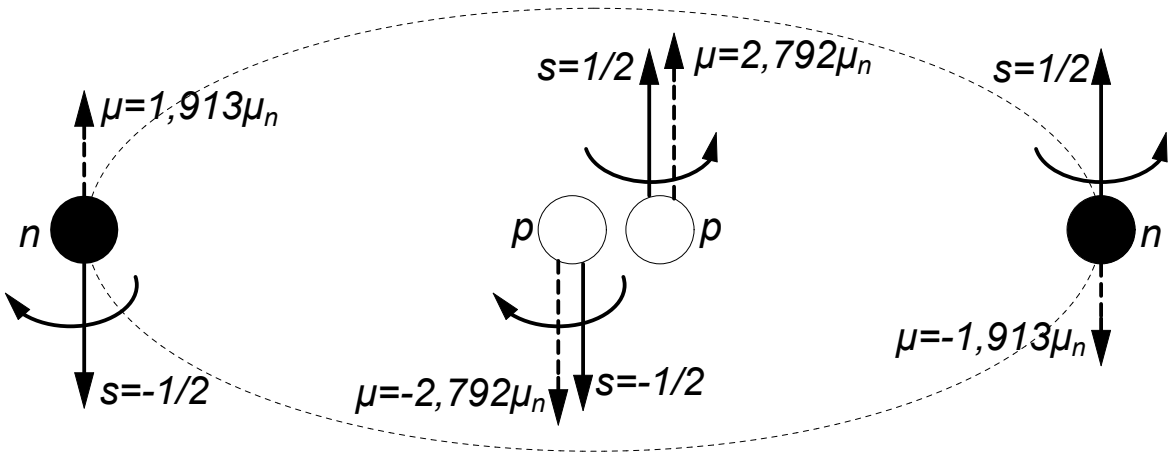

Figure 7. Structure model of helium nucleus $^4_2He = n+p+p+n$, with experimental spin $s = -1/2 - 1/2 + 1/2 + 1/2 = 0$ and with experimental magnetic moment $\mu = (1,913 + f)\mu_n - (2,792 + g)\mu_n + (2,792 + g)\mu_n - (1,913 + f)\mu_n = 0$. The mass defect $\Delta m = (14,11 + 14,11)MeV = 28,22$MeV is for the two neutrons only

The large mass defect $\Delta m = 14,11$MeV of each neutron is due to the very strong negativity of the inverse field. Therefore, the experimental mass defect of the helium nucleus ^4_2He is

$$\Delta m = (14,11 + 14,11)MeV = 28,22MeV \Rightarrow \Delta m = 28,22MeV. \tag{38}$$

It is noteworthy that, with helium ^4_2He, all the lower-order nuclei (^2_1H, ^3_1H, ^3_2He, ^4_2He) being the last, all the upper-order nuclei are constructed.

3. The Structure of the first upper-order Oxygen Nucleus $^{16}_{8}O$

3.1. Structure model of lithium nucleus $^{6}_{3}Li$

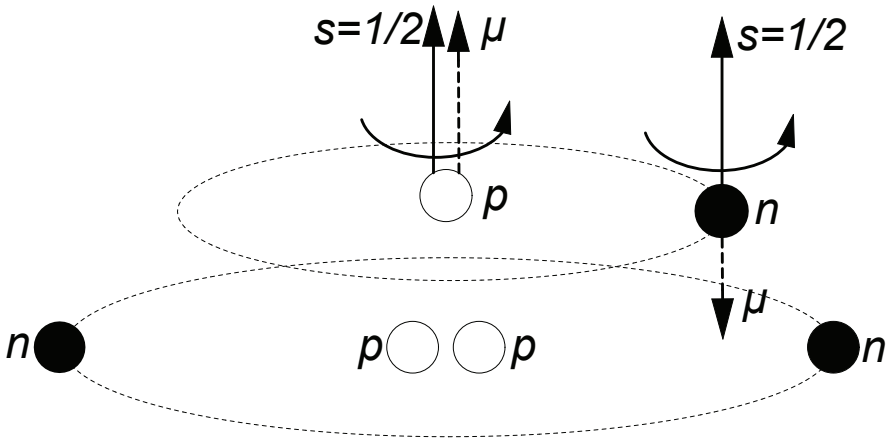

Figure 8. Structure model of lithium nucleus $^{6}_{3}Li =^{4}_{2} He +^{2}_{1} H$, with addition of one deuterium in the helium nucleus $^{4}_{2}He$

Lithium nucleus $^{6}_{3}Li$

$$^{6}_{3}Li =^{4}_{2} He +^{2}_{1} H \tag{39}$$

is derived from helium nucleus $^{4}_{2}He$ by addition of one deuterium $^{2}_{1}H$. Their protons are attracted by their common inverse electric field and are placed in a potential column.

The experimental spin is

$$s = 0 + 1 = 1 \Rightarrow s = 1 \tag{40}$$

and the experimental magnetic dipole moment is

$$\mu = 0 + (0,857 - 0,036)\mu_n = 0,821\mu_n \Rightarrow \mu = 0,821\mu_n, \tag{41}$$

where

$$\mu' = -0,036\mu_n \tag{42}$$

is the reduced magnetic moment of deuterium's proton, due to the interaction by the two protons of helium nucleus (interaction of same nucleons). It is reminded that the magnetic moment of $^{4}_{2}He$ is $\mu = 0$ (Eq. 37) and of $^{2}_{1}H$ is $\mu = 0,857\mu_n$ (Eq. 13).

The experimental mass defect of lithium nucleus $^{6}_{3}Li$ is

$$\Delta m = (28,22 + 1,52 - a) + (2,2 + a) = 31,94MeV, \tag{43}$$

where

$$\Delta m' = (1,52 - a)MeV \tag{44}$$

and

$$\Delta m'' = aMeV \tag{45}$$

are the increased mass defect of ${}^4_2He$ and ${}^2_1H$, due to the strong electric field of their protons. Also, it is reminded that the mass defect of ${}^4_2He$ is $\Delta m = 28,22\text{MeV}$ (Eq. 38) and of ${}^2_1H$ is $\Delta m = 2,2\text{MeV}$ (Eq. 16).

3.2. Structure model of lithium nucleus ${}^7_3Li$

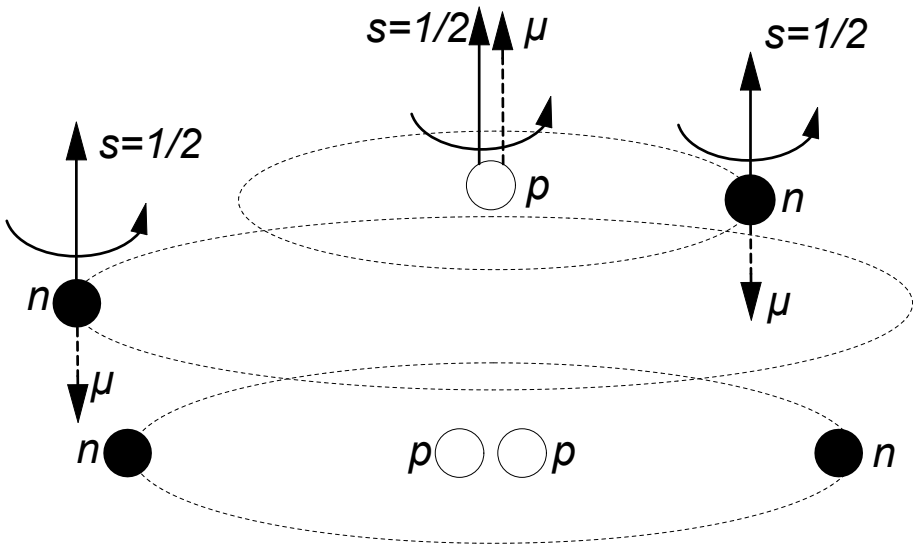

Figure 9. Structure model of lithium nucleus ${}^7_3Li = {}^4_2He + {}^2_1H + n$ or ${}^7_3Li = {}^6_3Li + n$, i.e. with addition of one bonding neutron in the lithium nucleus ${}^6_3Li$

Lithium nucleus ${}^7_3Li$ is created from lithium ${}^6_3Li$ by the insertion of one bonding neutron between helium ${}^4_2He$ and deuterium, due to the attraction of the negative potential column of their protons. The so-called bonding neutron reduces the strong negativity of the field and contributes to the stability of the nuclei, especially the heavier ones.

So, the lithium nucleus ${}^7_3Li$

$$ {}^7_3Li = {}^4_2He + {}^2_1H + n = {}^6_3Li + n \Rightarrow {}^7_3Li = {}^6_3Li + n \tag{46}$$

has an experimental spin

$$s = 0 + 1 + \frac{1}{2} = \frac{3}{2} \Rightarrow s = \frac{3}{2} \tag{47}$$

and an experimental magnetic dipole moment

$$\mu = 0 + (0,857 + 4,292 + a)\mu_n - (1,913 + a)\mu_n = 3,256\mu_n, \tag{48}$$

where

$$\mu' = (4,292 + a)\mu_n \tag{49}$$

is the increased magnetic moment of deuterium's proton, due to its interaction with the bonding neutron and

$$\mu'' = a\mu_n \tag{50}$$

is the increased magnetic moment of bonding neutron. It is reminded that the magnetic moment of ${}^4_2He$ is $\mu = 0$ and of ${}^2_1H$ is $\mu = 0,857\mu_n$.

The experimental mass defect of lithium nucleus ${}^7_3Li$ is calculated

$$\Delta m = (28,22 + c) + (2,2 + b) + (2,2 + 5,55 - c - b) = 38,17MeV. \quad (51)$$

Also, it is reminded that the mass defect of ${}^4_2He$ is $\Delta m = 28,22$MeV and of ${}^2_1H$ (or of the bonding neutron) is $\Delta m = 2,2$MeV.

3.3. Structure model of beryllium nucleus ${}^8_4Be$

Beryllium nucleus ${}^8_4Be$

$${}^8_4Be =^4_2 H_e +^4_2 He \quad (52)$$

is derived from two helium nuclei, ${}^4_2He$, and is an unstable nucleus that breaks down into two ${}^4_2He$ nuclei (alpha particles) via alpha decay. It is important to note the role of orbital bonding neutrons in stabilizing nuclei. The beryllium nucleus lacks these neutrons, resulting in a strong negativity of the field and instability.

3.4. Structure model of beryllium nucleus ${}^9_4Be$

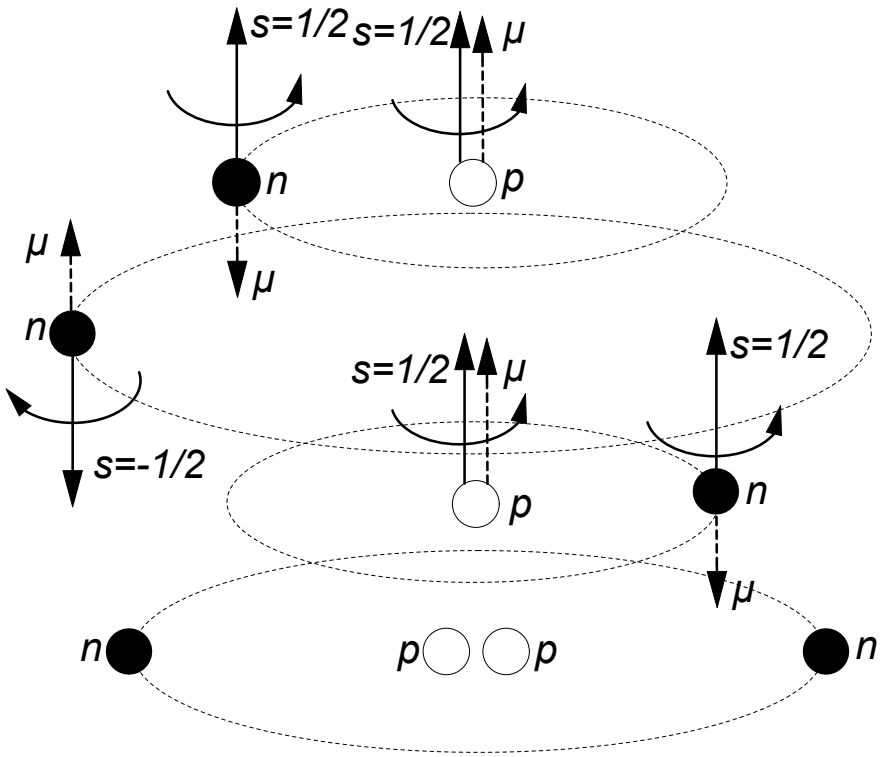

Figure 10. Structure model of beryllium nucleus ${}^9_4Be =^4_2 He + 2^2_1H + n$, with addition of two deuterium nuclei ${}^2_1H$ and one bonding neutron in the helium nucleus ${}^4_2He$

Beryllium nucleus ${}^{9}_{4}Be$ is derived from one helium nucleus ${}^{4}_{2}He$, two deuterium nuclei ${}^{2}_{1}H$ and one bonding neutron (Fig. 10)

$$ {}^{9}_{4}Be = {}^{4}_{2}He + {}^{2}_{1}H + n + {}^{2}_{1}H \tag{53} $$

and has an experimental spin

$$ s = 0 + 1 - \frac{1}{2} + 1 = \frac{3}{2} \Rightarrow s = \frac{3}{2} \tag{54} $$

and an experimental magnetic dipole moment (see Eqs 13 and 37)

$$ \mu = 0 + (0,857 - a)\mu_n - (1,913 + 0,978)\mu_n + (0,857 + a)\mu_n = -1,177\mu_n. \tag{55} $$

The increased mass defect of beryllium nucleus ${}^{9}_{4}Be$ is calculated (see Eqs 16 and 38)

$$ \Delta m = 28,22 + (2,2 + 12) + 13,49 + (2,2 - 0,2) = 60,11MeV \tag{56} $$

It is noted that possible fluctuations were considered in the equations of the magnetic moment and mass defect. Specifically, the lower deuterium, adjacent to the protons of helium ${}^{4}_{2}He$ (Fig. 10), has a reduced magnetic moment and an increased mass defect, while the upper deuterium, adjacent to the neutron, exhibits opposite fluctuations (see subsection 1.4).

3.5. Structure model of boron nucleus ${}^{10}_{5}B$

Boron nucleus ${}^{10}_{5}B$ is derived from one helium ${}^{4}_{2}He$ and three deuterium nuclei ${}^{2}_{1}H$, whose the sum of their spins gives $s = 3$ and so (Fig. 11)

$$ {}^{10}_{5}B = {}^{4}_{2}He + {}^{2}_{1}H + {}^{2}_{1}H + {}^{2}_{1}H \tag{57} $$

has an experimental spin

$$ s = 0 + 1 + 1 + 1 = 3 \Rightarrow s = 3 \tag{58} $$

and an experimental magnetic dipole moment

$$ \mu = 0 + 3(0,857 - 0,257)\mu_n = 1,8\mu_n \Rightarrow \mu = 1,8\mu_n, \tag{59} $$

where

$$ \mu' = -3 \cdot 0,257\mu_n \tag{60} $$

is the reduced magnetic moment of the three deuterium's protons, due to their interaction.

The mass defect of the boron nucleus ${}^{10}_{5}B$ is calculated

$$ \Delta m = 28,22 + 3 \cdot 12,14 = 64,65MeV \Rightarrow \Delta m = 64,65MeV, \tag{61} $$

namely it is equal to the mass defect of helium ${}^{4}_{2}He$ ($\Delta m = 28,22$MeV) and to the increased mass defect of the three deuterium nuclei ($\Delta m = 3 \cdot 12,14$MeV), whose their orbital neutrons are near to the very strong electric field of the protons.

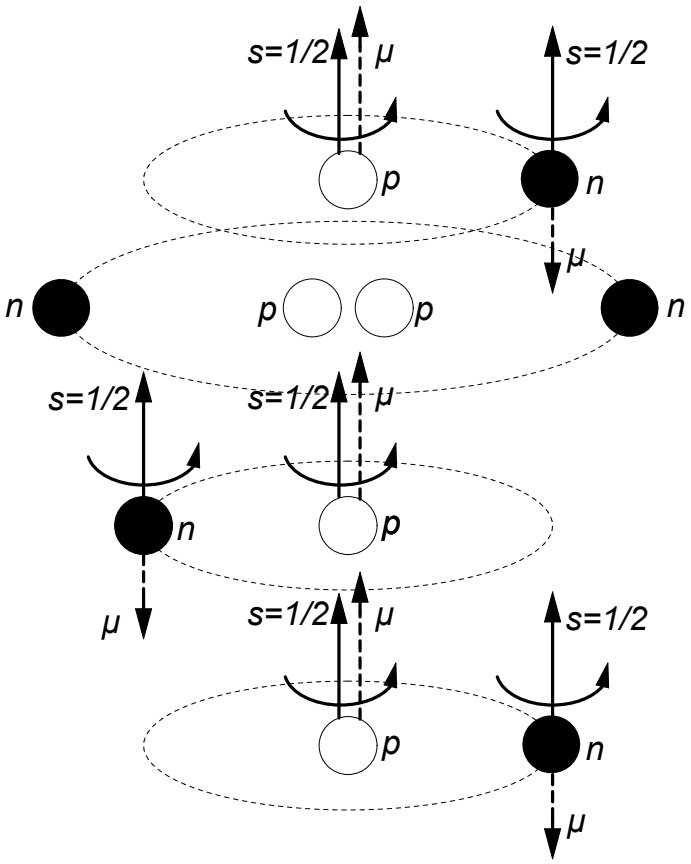

Figure 11. Structure model of boron nucleus ${}^{10}_{5}B = {}^{4}_{2}He + 3{}^{2}_{1}H$, with addition of three deuterium nuclei ${}^{2}_{1}H$ in the helium nucleus ${}^{4}_{2}He$

3.6. Structure model of boron nucleus ${}^{11}_{5}B$

Boron nucleus ${}^{11}_{5}B$ is derived from one helium ${}^{4}_{2}He$, one helium ${}^{3}_{2}He$, one tritium ${}^{3}_{1}H$ and one bonding neutron, whose the sum of their spins gives $s = 3/2$ and so (Fig. 12)

$$ {}^{11}_{5}B = {}^{4}_{2}He + {}^{3}_{2}He + {}^{3}_{1}H + n \tag{62}$$

has an experimental spin

$$ s = 0 + \frac{1}{2} + \frac{1}{2} + \frac{1}{2} = \frac{3}{2} \Rightarrow s = \frac{3}{2} \tag{63}$$

and an experimental magnetic dipole moment

$$ \mu = 0 + (-2,127 + 1,25) + (2,978 + 1,25) + (-1,913 + 1,25) = 2,688\mu_n \tag{64}$$

The experimental mass defect of the boron nucleus ${}^{11}_{5}B$ is calculated

$$ \Delta m = 28,22 + (7,69 + 6,7) + (8,48 + 10) + (2,2 + 12,8) = 76,09 MeV. \tag{65}$$

It is noted that, the possible fluctuations were considered into the equations of the magnetic moment and mass defect.

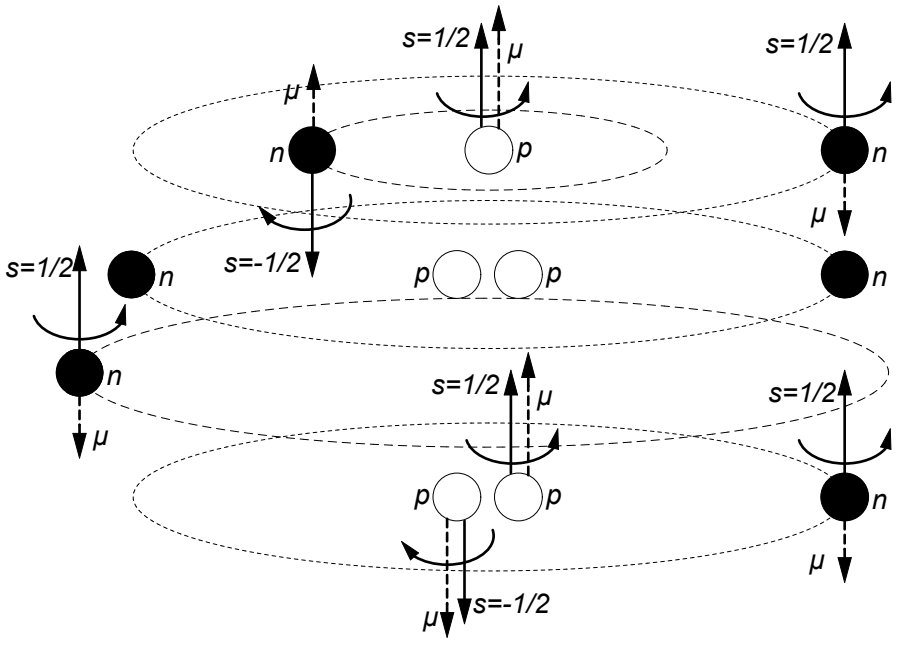

Figure 12. Structure model of boron nucleus ${}^{11}_{5}B =^{4}_{2} He +^{3}_{2} He +^{3}_{1} H + n$, with addition of one helium ${}^{3}_{2}He$, one tritium ${}^{3}_{1}H$ and one bonding neutron in the helium ${}^{4}_{2}He$

3.7. Structure model of carbon nucleus ${}^{12}_{6}C$

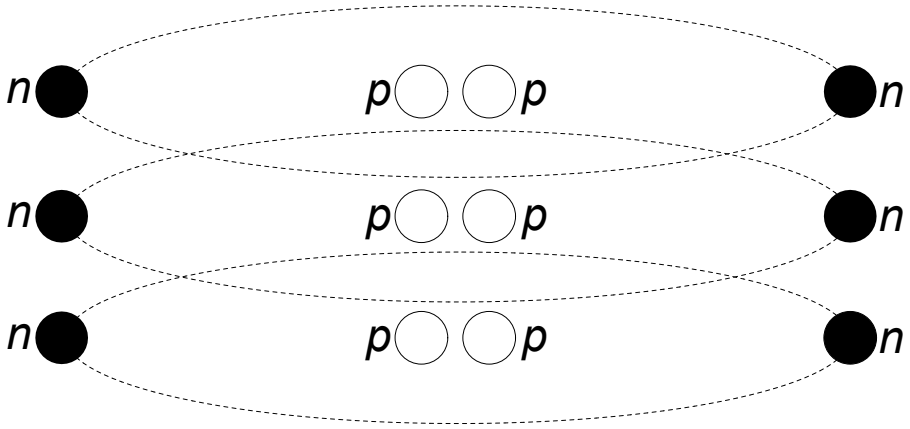

Figure 13. Structure model of carbon nucleus ${}^{12}_{6}C = 3^{4}_{2}He$, as a column strong electric field of three coaxial helium nuclei ${}^{4}_{2}He$

Carbon nucleus ${}^{12}_{6}C$ is derived from three helium nuclei ${}^{4}_{2}He$ and is a stable nucleus but not an upper-order one and so its atomic number $Z = 6$ is not a "magic number" either and so

$$ {}^{12}_{6}C =^{4}_{2} He +^{4}_{2} He +^{4}_{2} He. \tag{66}$$

Their protons are attracted by their common inverse electric field and placed in a

potential column. So, the experimental spin of the carbon nucleus ${}^{12}_{6}C$ is

$$s = 0 + 0 + 0 = 0 \Rightarrow s = 0 \tag{67}$$

and its experimental magnetic dipole moment is

$$\mu = 0 + 0 + 0 = 0 \Rightarrow \mu = 0. \tag{68}$$

The experimental mass defect of the carbon nucleus is calculated

$$\Delta m = 28,22 + 3 \cdot 7,38 = 92,04MeV \Rightarrow \Delta m = 92,04MeV, \tag{69}$$

namely it is equal to the mass defect of helium ${}^{4}_{2}He$ ($\Delta m = 28,22$MeV) and to the equal increase the mass defect of the three helium nuclei ${}^{4}_{2}He$ ($\Delta m = 3 \cdot 7,38$MeV).

3.8. Structure model of nitrogen nucleus ${}^{14}_{7}N$

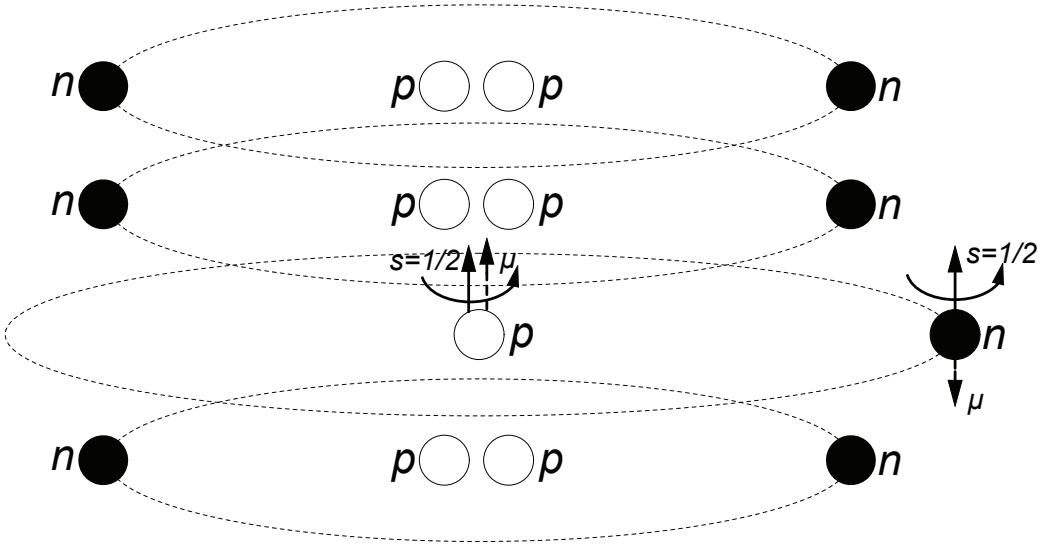

Figure 14. Structure model of nitrogen nucleus ${}^{14}_{7}N = {}^{12}_{6}C + {}^{2}_{1}H$, with addition of one deuterium ${}^{2}_{1}H$ in the carbon ${}^{12}_{6}C$

Nitrogen nucleus ${}^{14}_{7}N$ is derived from one carbon ${}^{12}_{6}C$ with addition of one deuterium ${}^{2}_{1}H$, whose the spin is $s = 1$ and so

$${}^{14}_{7}N = {}^{12}_{6}C + {}^{2}_{1}H \tag{70}$$

has an experimental spin

$$s = 0 + 1 = 1 \Rightarrow s = 1 \tag{71}$$

and an experimental magnetic dipole moment

$$\mu = 0 + (0,857 - 0,454)\mu_n = 0,403\mu_n \Rightarrow \mu = 0,403\mu_n, \tag{72}$$

where

$$\mu' = -0,454\mu_n \tag{73}$$

is the reduced magnetic moment of the deuterium's proton (interaction of same nucleons).

The increased mass defect is due to the reduced magnetic moment. So, the mass defect of the nitrogen nucleus $^{14}_{7}N$ is calculated (Eqs 16 and 69)

$$\Delta m = 92,04 + (2,2 + 10,2) = 104,5MeV \Rightarrow \Delta m = 104,5MeV. \quad (74)$$

3.9. Structure model of oxygen nucleus $^{16}_{8}O$

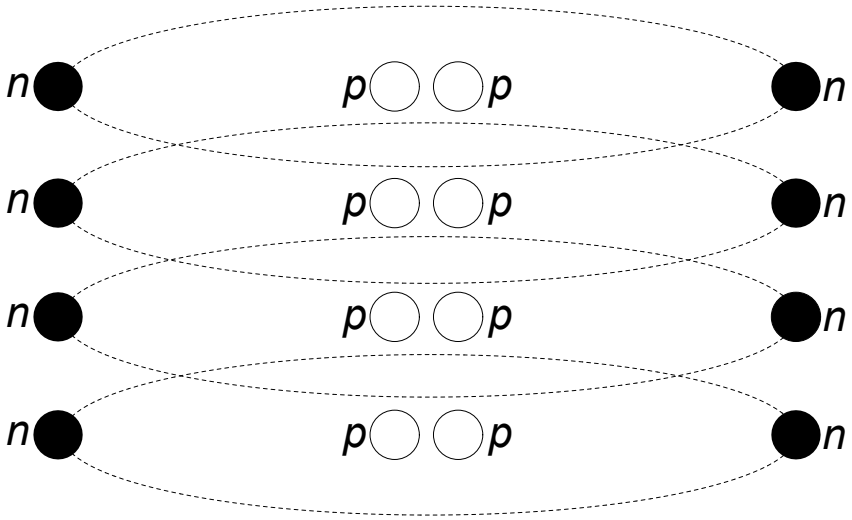

Figure 15. Structure model of oxygen nucleus $^{16}_{8}O = 4^{4}_{2}He$, as a column strong electric field of four coaxial helium nuclei $^{4}_{2}He$

Oxygen nucleus $^{16}_{8}O$ is derived from the nitrogen nucleus $^{14}_{7}N$ (Eq. 70) by completing of the deuterium $^{2}_{1}H$ as a helium $^{4}_{2}He$ and so

$$^{16}_{8}O =^{12}_{6} C +^{4}_{2} He \quad (75)$$

has an experimental spin

$$s = 0 + 0 = 0 \Rightarrow s = 0 \quad (76)$$

and an experimental magnetic dipole moment

$$\mu = 0 + 0 = 0 \Rightarrow \mu = 0. \quad (77)$$

The experimental mass defect of the oxygen nucleus is calculated

$$\Delta m = 92,04 + (28,22 + 7,2) = 127,46MeV \Rightarrow \Delta m = 127,46MeV, \quad (78)$$

where

$$\Delta m' = 7,2MeV \quad (79)$$

is a small increase of the magnetic moment, due to the increased negativity of the field. It is noted that, $\Delta m = 92,04$MeV (Eq. 69) and $\Delta m = 28,22$MeV (Eq. 38) are the respective mass defects of carbon $^{12}_{6}C$ and helium $^{4}_{2}He$.

After the helium nucleus ${}^{4}_{2}He$, the oxygen nucleus ${}^{16}_{8}O$ is the second stable one in nature and the first upper-order nucleus. From this first upper-order nucleus, the second one is constructed (calcium nucleus ${}^{40}_{20}Ca$) and from the second, the third one (tin nucleus ${}^{120}_{50}Sn$), according to mirror symmetry.

4. The Structure of the second upper-order Calcium Nucleus ${}^{40}_{20}Ca$

4.1. Structure model of fluorine nucleus ${}^{19}_{9}F$

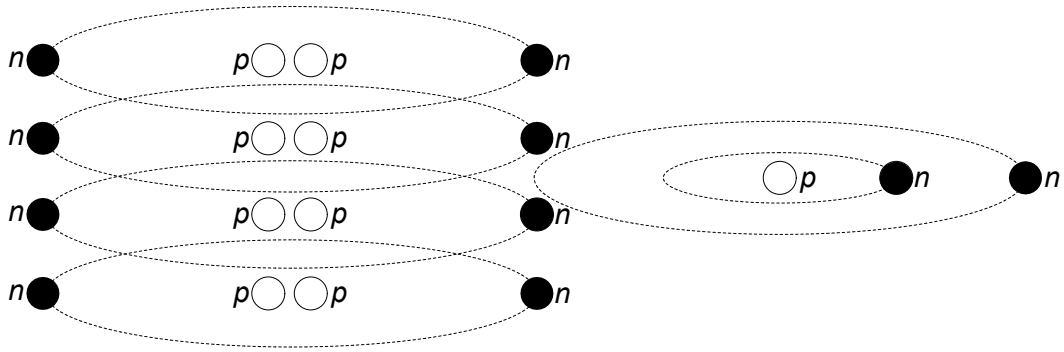

Figure 16. Structure model of fluorine nucleus ${}^{19}_{9}F = {}^{16}_{8}O + {}^{3}_{1}H$, with addition of one tritium nucleus ${}^{3}_{1}H$ adjacent to an oxygen nucleus ${}^{16}_{8}O$

Fluorine nucleus ${}^{19}_{9}F$

$$ {}^{19}_{9}F = {}^{16}_{8}O + {}^{3}_{1}H \tag{80}$$

is derived by addition of one tritium nucleus ${}^{3}_{1}H$ adjacent to an oxygen nucleus ${}^{16}_{8}O$.

The experimental spin is

$$ s = 0 + \frac{1}{2} = \frac{1}{2} \Rightarrow s = \frac{1}{2} \tag{81}$$

and the experimental magnetic dipole moment is

$$ \mu = 0 + (2,978 - 0,351)\mu_n = 2,627\mu_n \Rightarrow \mu = 2,627\mu_n, \tag{82}$$

where

$$ \mu' = -0,351\mu_n \tag{83}$$

is the reduced magnetic moment of tritium's proton, due to the interaction by the protons of oxygen nucleus. It is reminded that the magnetic moment of ${}^{16}_{8}O$ is $\mu = 0$ and of ${}^{3}_{1}H$ is $\mu = 2,978\mu_n$ (Eq. 20).

The experimental mass defect of fluorine nucleus ${}^{19}_{9}F$, due to the reduced magnetic moment, is

$$ \Delta m = 127,46 + (8,48 + 11,95) = 147,89MeV, \tag{84}$$

where

$$ \Delta m' = 11,95MeV \tag{85}$$

is the increased mass defect of ${}^{3}_{1}H$, due to the electric field of the oxygen's protons. Also, it is reminded that the mass defect of ${}^{16}_{8}O$ is $\Delta m = 127,46\text{MeV}$ (Eq. 78) and of ${}^{3}_{1}H$ is $\Delta m = 8,48\text{MeV}$ (Eq. 24).

4.2. Structure model of magnesium nucleus ${}^{24}_{12}Mg$

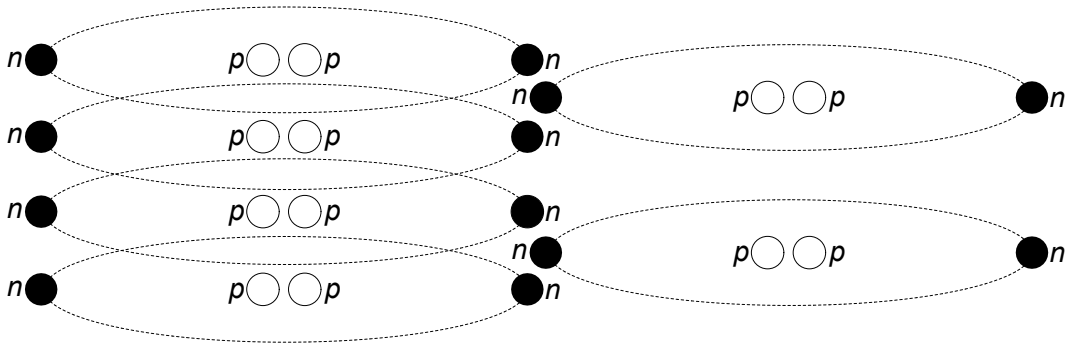

Figure 17. Structure model of magnesium nucleus ${}^{24}_{12}Mg = {}^{16}_{8}O + 2{}^{4}_{2}He$, with addition of two helium nuclei ${}^{4}_{2}He$ adjacent to an oxygen nucleus ${}^{16}_{8}O$

Magnesium nucleus ${}^{24}_{12}Mg$

$$ {}^{24}_{12}Mg = {}^{16}_{8}O + 2{}^{4}_{2}He \tag{86} $$

is derived by addition of two helium nuclei ${}^{4}_{2}He$ adjacent to an oxygen nucleus ${}^{16}_{8}O$.

The experimental spin is

$$ s = 0 + 0 = 0 \Rightarrow s = 0 \tag{87} $$

and the experimental magnetic dipole moment is

$$ \mu = 0 + 0 = 0 \Rightarrow \mu = 0. \tag{88} $$

The experimental mass defect of magnesium nucleus ${}^{24}_{12}M_g$ is

$$ \Delta m = 127,46 + (2 \cdot 28,22 + 14,11) = 198,01MeV, \tag{89} $$

where

$$ \Delta m' = 14,11MeV \tag{90} $$

is the increased mass defect of the two ${}^{4}_{2}He$, due to the electric field of the oxygen's protons. Also, it is reminded that the mass defect of ${}^{16}_{8}O$ is $\Delta m = 127,46\text{MeV}$ and of ${}^{4}_{2}He$ is $\Delta m = 28,22\text{MeV}$.

4.3. Structure model of silicon nucleus ${}^{28}_{14}Si$

Silicon nucleus ${}^{28}_{14}Si$ (Fig. 18)

$$ {}^{28}_{14}Si = {}^{16}_{8}O + 3{}^{4}_{2}He \tag{91} $$

is derived by addition of three helium nuclei ${}^{4}_{2}He$ adjacent to an oxygen nucleus ${}^{16}_{8}O$.

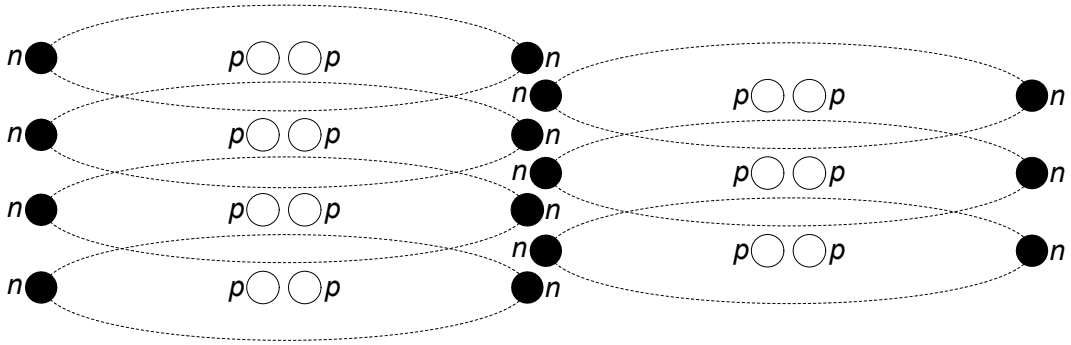

Figure 18. Structure model of silicon nucleus $^{28}_{14}Si =^{16}_{8} O + 3^{4}_{2}He$, with addition of three helium nuclei $^{4}_{2}He$ adjacent to an oxygen nucleus $^{16}_{8}O$

The experimental spin is

$$s = 0 + 0 = 0 \Rightarrow s = 0 \tag{92}$$

and the experimental magnetic dipole moment is

$$\mu = 0 + 0 = 0 \Rightarrow \mu = 0. \tag{93}$$

The experimental mass defect of silicon nucleus $^{28}_{14}S_i$ is

$$\Delta m = 127,46 + (3 \cdot 28,22 + 24,13) = 236,25MeV, \tag{94}$$

where

$$\Delta m' = 24,13MeV \tag{95}$$

is the increased mass defect. Also, it is reminded that the mass defect of $^{16}_{8}O$ is $\Delta m = 127,46$MeV and of $^{4}_{2}He$ is $\Delta m = 28,22$MeV.

4.4. Structure model of calcium nucleus $^{40}_{20}Ca$

Calcium nucleus $^{40}_{20}Ca$ (Fig. 19)

$$^{40}_{20}Ca =^{16}_{8} O + 2^{4}_{2}He +^{16}_{8} O \tag{96}$$

is derived of two oxygen nuclei $^{16}_{8}O$ by bonding adjacent of two helium nuclei $^{4}_{2}He$ (a half oxygen), according to the mirror symmetry (2.5 factor).

The experimental spin is

$$s = 0 + 0 = 0 \Rightarrow s = 0 \tag{97}$$

and the experimental magnetic dipole moment is

$$\mu = 0 + 0 = 0 \Rightarrow \mu = 0. \tag{98}$$

The experimental mass defect of calcium nucleus $^{40}_{20}Ca$ is

$$\Delta m = 127,46 + (2 \cdot 28,22 + 30) + 127,46 = 341,35MeV, \tag{99}$$

where

$$\Delta m' = 30MeV \tag{100}$$

is the increased mass defect of the two ${}^{4}_{2}He$, due to the electric field of the oxygen's protons. Also, it is reminded that the mass defect of ${}^{16}_{8}O$ is $\Delta m = 127,46\text{MeV}$ and of ${}^{4}_{2}He$ is $\Delta m = 28,22\text{MeV}$.

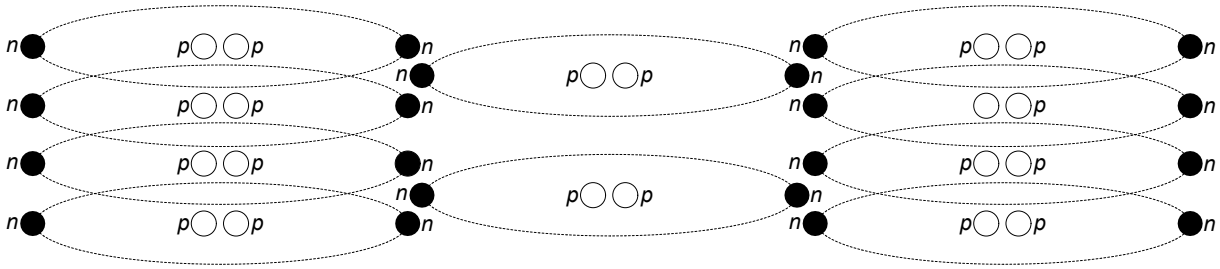

Figure 19. Structure model of calcium nucleus ${}^{40}_{20}Ca = {}^{16}_{8}O + 2{}^{4}_{2}He + {}^{16}_{8}O$, as a mirror symmetry of two oxygen nuclei ${}^{16}_{8}O$ and two helium nuclei ${}^{4}_{2}He$ (a half oxygen), according to the $2,5$ factor

After the oxygen nucleus ${}^{16}_{8}O$, which is the first upper-order nucleus, the calcium nucleus ${}^{40}_{20}Ca$ is the second one. From this second upper-order nucleus, the third one is constructed (tin nucleus ${}^{120}_{50}Sn$), and from the third, the basis for the structure of all heavy nuclei up to the radioactive uranium nucleus ${}^{235}_{92}U$ is formed.

5. The Structure of the third upper-order Tin Nucleus ${}^{120}_{50}Sn$

5.1. Structure model of iron nucleus ${}^{56}_{26}Fe$

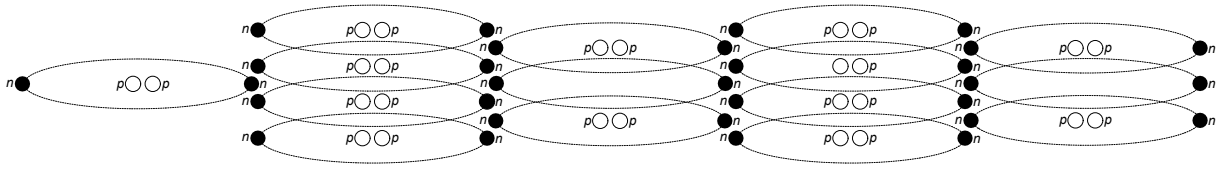

Figure 20. Structure model of iron nucleus ${}^{56}_{26}Fe = {}^{40}_{20}Ca + 3{}^{4}_{2}He + 4n$, with addition of two helium nuclei ${}^{4}_{2}He$ and one ${}^{4}_{2}He$ adjacent to a calcium nucleus ${}^{40}_{20}Ca$, while four bonding neutrons are added

Iron nucleus ${}^{56}_{26}Fe$

$$ {}^{56}_{26}Fe = {}^{40}_{20}Ca + 3{}^{4}_{2}He + 4n \tag{101} $$

is derived by addition of two helium nuclei ${}^{4}_{2}He$ and one ${}^{4}_{2}He$ adjacent to a calcium nucleus ${}^{40}_{20}Ca$, while four bonding neutrons are added, which reduce the strong negativity of the protons field and contribute to the stability of the nucleus.

The experimental spin is

$$ s = 0 + 0 + 0 = 0 \Rightarrow s = 0 \tag{102} $$

and the experimental magnetic dipole moment is

$$ \mu = 0 + 0 + 0 = 0 \Rightarrow \mu = 0. \tag{103} $$

The experimental mass defect of iron nucleus $^{56}_{26}Fe$ is

$$\Delta m = 341,35 + (3 \cdot 28,22 + 7,39) + 4 \cdot (2,2 + 12,37) = 491,68 MeV, \quad (104)$$

where

$$\Delta m' = 7,39 MeV \quad (105)$$

is the increased mass defect of the three helium nuclei $^{4}_{2}He$, due to the electric field of the calcium's protons. Also, it is reminded that the mass defect of $^{40}_{20}Ca$ is $\Delta m = 341,35$MeV (Eq. 99), of $^{4}_{2}H_e$ is $\Delta m = 28,22$MeV and of the bonding neutron is $\Delta m = 2,2$MeV.

5.2. Structure model of nickel nucleus $^{60}_{28}Ni$

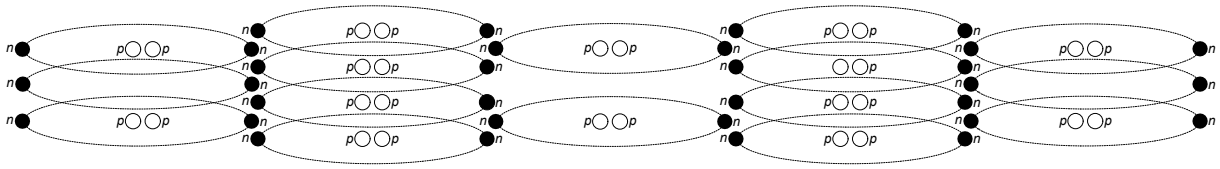

Figure 21. Structure model of nickel nucleus $^{60}_{28}Ni =^{40}_{20} Ca + 4^{4}_{2}He + 4n$, with addition of two helium nuclei $^{4}_{2}He$ and two $^{4}_{2}He$ adjacent to a calcium nucleus $^{40}_{20}Ca$, while four bonding neutrons are added

Nickel nucleus $^{60}_{28}Ni$

$$^{60}_{28}Ni =^{40}_{20} Ca + 4^{4}_{2}He + 4n \quad (106)$$

is derived by addition of two helium nuclei $^{4}_{2}He$ and two $^{4}_{2}He$ adjacent to a calcium nucleus $^{40}_{20}Ca$, while four bonding neutrons are added, which reduce the strong negativity of the protons field and contribute to the stability of the nucleus.

The experimental spin is

$$s = 0 + 0 + 0 = 0 \Rightarrow s = 0 \quad (107)$$

and the experimental magnetic dipole moment is

$$\mu = 0 + 0 + 0 = 0 \Rightarrow \mu = 0. \quad (108)$$

The experimental mass defect of nickel nucleus $^{60}_{28}Ni$ is

$$\Delta m = 341,35 + (4 \cdot 28,22 + 7,39) + 4 \cdot (2,2 + 13,95) = 526,23 MeV, \quad (109)$$

where

$$\Delta m' = 7,39 MeV \quad (110)$$

is the increased mass defect of the four $^{4}_{2}H_e$, due to the electric field of the calcium's protons. Also, it is reminded that the mass defect of $^{40}_{20}C_a$ is $\Delta m = 341,35$MeV, of $^{4}_{2}H_e$ is $\Delta m = 28,22$MeV and of the bonding neutron is $\Delta m = 2,2$MeV.

5.3. Structure model of tin nucleus $^{120}_{50}Sn$

The tin nucleus $^{120}_{50}S_n$ (Figs 22 and 23)

$$^{120}_{50}S_n = ^{40}_{20}C_a + \frac{1}{2}\cdot ^{40}_{20}C_a + ^{40}_{20}C_a + 20n, \tag{111}$$

is constructed by repeating the calcium nucleus $^{40}_{20}C_a$ and half of it for connection as the third upper-order nucleus, according to mirror symmetry (a 2.5 factor). Twenty orbital bonding neutrons are added, which reduce the strong negativity of the proton field and contribute to the stability of the nucleus.

In Fig.22, the same image is repeated on the other three sides of the rectangular parallelepiped, while the lone helium nucleus $^{4}_{2}He$ from the above figure is placed in its center. In Fig.23, four corner columns of negative potential appear with four helium nuclei $^{4}_{2}He$ and three neutrons each. Additionally, four middle columns of negative potential appear with two helium nuclei $^{4}_{2}He$ and two neutrons each, while the lone helium nucleus $^{4}_{2}He$ appears in the center.

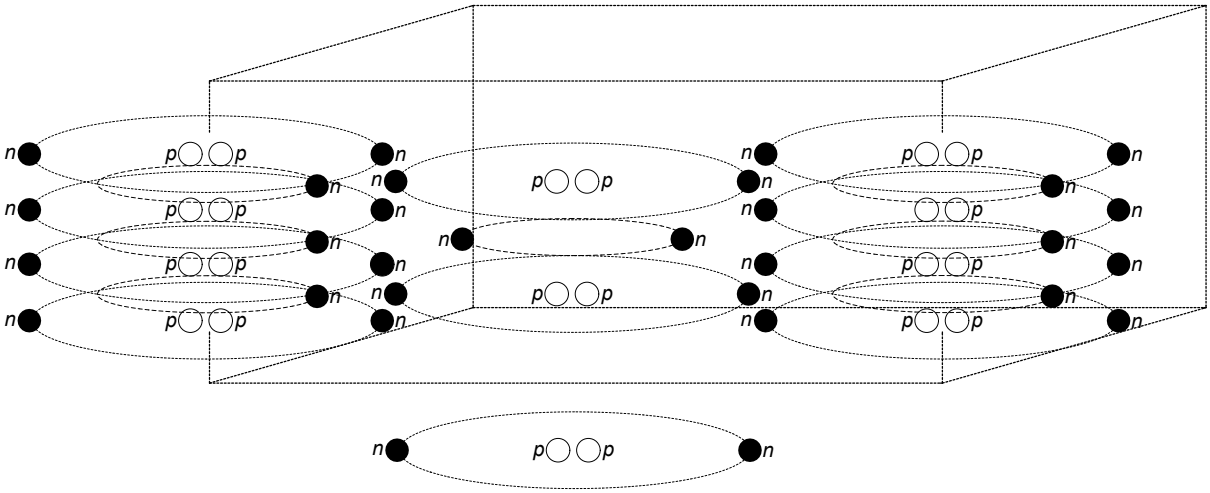

Figure 22. Stereoscopic representation of the tin nucleus $^{120}_{50}Sn$, where the same image is repeated on the other three sides of the rectangular parallelepiped, while the lone helium nucleus $^{4}_{2}He$ is placed at its center

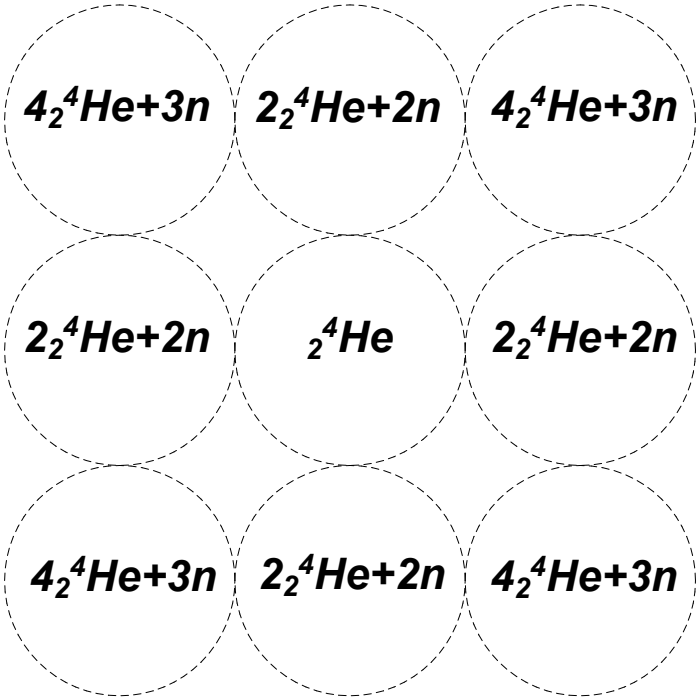

Figure 23. Top view of Fig. 22, where the mirror symmetry of the 2.5 factor appears in the construction of the tin nucleus $^{120}_{50}Sn$

The experimental spin is

$$s = 0 + 0 + 0 = 0 \Rightarrow s = 0 \tag{112}$$

and the experimental magnetic dipole moment is

$$\mu = 0 + 0 + 0 = 0 \Rightarrow \mu = 0. \tag{113}$$

The experimental mass defect of tin nucleus $^{120}_{50}Sn$ is (see Eq. **??**)

$$\Delta m = 341,35 + \frac{1}{2} \cdot 341,35 + 341,35 + 20 \cdot (2,2 + 6,1) = 1019,31 MeV. \tag{114}$$

Also, it is reminded that the mass defect of $^{40}_{20}Ca$ is $\Delta m = 341,35$MeV (Eq. 99) and of the bonding neutron is $\Delta m = 2,2$MeV.

After the nuclei of oxygen $^{16}_{8}O$ and calcium $^{40}_{20}Ca$, which are the first and second upper-order ones, the tin nucleus $^{120}_{50}Sn$ is the third upper-order nucleus. From this third upper-order nucleus, the fourth one is the hypothetical construct (orion nucleus $^{307}_{125}Or$), as forecasted by the unified theory of dynamic space.[3] It is noted that the word "orion" comes from the Greek *όριον*, meaning "the limit". Thus, orion nucleus $^{307}_{125}Or$ means the limited nucleus of nature that cannot be further divided, due to the indivisible original deuterium.

The atomic numbers[6] Z of the above four upper-order nuclei are the so-called four "magic numbers", i.e., $Z_1 = 8$, $Z_2 = 8 \cdot 2.5 = 20$, $Z_3 = 20 \cdot 2.5 = 50$, and $Z_4 = 50 \cdot 2.5 = 125$, according to the mirror symmetry. It is noted that this orion nucleus $^{307}_{125}Or$ with an atomic number $Z_4 = 125$ is the corresponding "hypothetical

unbihexium Ubh", whose different atomic number is $Z = 126$. However, the number $Z_4 = 125$ looks symmetrical and not magical at all, due to the 2.5 factor.

6. Structure of the Uranium Nucleus $^{235}_{92}U$

6.1. Structure model of iodine nucleus $^{127}_{53}I$

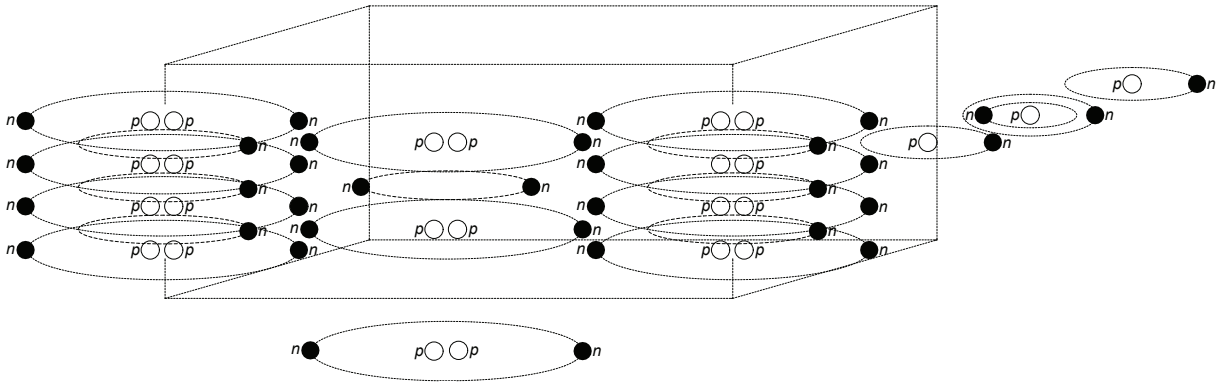

Figure 24. Stereoscopic representation of the iodine nucleus $^{127}_{53}I$, where the addition of two deuterium nuclei $^{2}_{1}H$ and one tritium nucleus $^{3}_{1}H$ appears adjacent to the side of a tin nucleus $^{120}_{50}Sn$ (Figs 22 and 23)

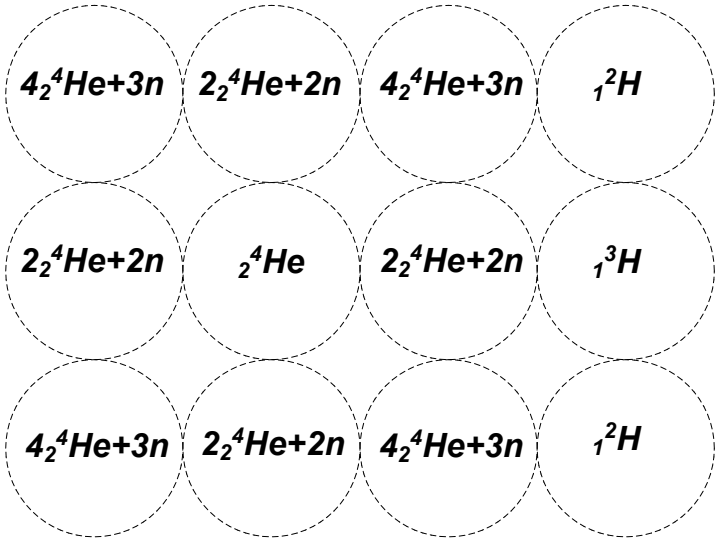

Figure 25. Top view of Fig. 24, where the mirror symmetry of the 2,5 factor of the tin nucleus $^{120}_{50}Sn$ appears, while the iodine nucleus $^{127}_{53}I$ is constructed from the addition of two deuterium nuclei $^{2}_{1}H$ and one tritium nucleus $^{3}_{1}H$

Iodine nucleus $^{127}_{53}I$ (Figs 24 and 25)

$$^{127}_{53}I =^{120}_{50} Sn + 2^{2}_{1}H +^{3}_{1} H \tag{115}$$

is constructed from the addition of two deuterium nuclei and one tritium, adjacent onto the side of a tin nucleus $^{120}_{50}Sn$.

The experimental spin is

$$s = 0 + 2 \cdot 1 + \frac{1}{2} = \frac{5}{2} \Rightarrow s = \frac{5}{2} \tag{116}$$

and the experimental magnetic dipole moment is (Eq. 115)

$$\mu = 0 + 2(0,857 - a) + (2,978 - 1,898 + 2a) = 2,794\mu_n \Rightarrow \mu = 2,794\mu_n, \tag{117}$$

where the reduced magnetic moment of deuterium and tritium is due to the strong negative electric field. It is reminded that the magnetic moment of tin, deuterium and tritium is $\mu = 0$, $\mu = 0,857\mu_n$ and $\mu = 2,978\mu_n$ respectively.

The experimental mass defect of iodine nucleus ${}^{127}_{53}I$ is (Eq. 115)

$$\Delta m = 1019,31 + 2(2,2 + 10) + (8,48 + 19,07) = 1071,26MeV, \tag{118}$$

where the increased mass defect of deuterium and tritium is due to the strong negative electric field. Also, it is reminded that the mass defect of tin, deuterium and tritium is $\Delta m = 1019$MeV, $\Delta m = 2,2$MeV and $\Delta m = 8,48$MeV respectively.

6.2. Structure model of lead nucleus ${}^{208}_{82}Pb$

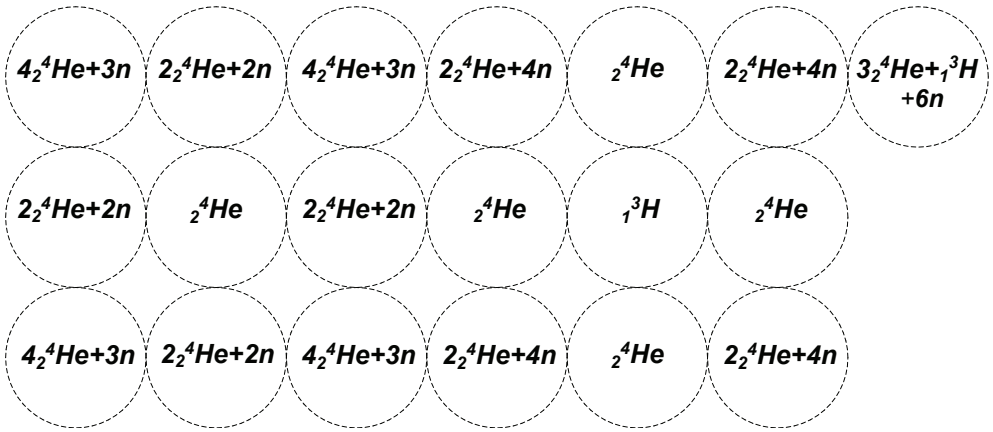

Figure 26. Representation of the lead nucleus ${}^{208}_{82}Pb$, where the addition of three helium nuclei ${}^4_2He$, one tritium nucleus ${}^3_1H$, and six bonding neutrons appears adjacent to the corner potential column of the rhenium nucleus ${}^{187}_{75}Re$

Lead nucleus ${}^{208}_{82}Pb$

$${}^{208}_{82}Pb = {}^{120}_{50}Sn + \frac{1}{2} \cdot {}^{120}_{50}Sn + 3{}^4_2He + {}^3_1H + 6n + 6n + n \tag{119}$$

is constructed by one tin nucleus ${}^{120}_{50}Sn$, a half of it, three helium nuclei ${}^4_2He$, one tritium nucleus ${}^3_1H$ and thirteen bonding neutrons.

However, the rhenium nucleus ${}^{187}_{75}Re$ (as shown in Figure 26, i.e. excludes the three helium nuclei ${}^4_2He$, one tritium nucleus ${}^3_1H$, and six neutrons)

$${}^{187}_{75}Re = {}^{120}_{50}Sn + \frac{1}{2} \cdot {}^{120}_{50}Sn + 6n + n \tag{120}$$

involves one tin nucleus $^{120}_{50}Sn$, half of another tin nucleus, and six bonding neutrons. One additional neutron is added to form the deuterium nucleus $^{2}_{1}H$ (half $^{4}_{2}He$), which evolves into the tritium nucleus $^{3}_{1}H$.

For lead nucleus $^{208}_{82}Pb$ (Fig. 26) Eq. 119, due to Eq. 120, is written

$$^{208}_{82}Pb =^{187}_{75} Re + 3^{4}_{2}He +^{3}_{1} H + 6n. \tag{121}$$

Thus, it is constructed from the addition of three helium nuclei $^{4}_{2}He$, one tritium nucleus $^{3}_{1}H$, and six bonding neutrons adjacent to the corner potential column of the rhenium nucleus $^{187}_{75}Re$.

6.3. Structure model of bismuth nucleus $^{209}_{83}Bi$

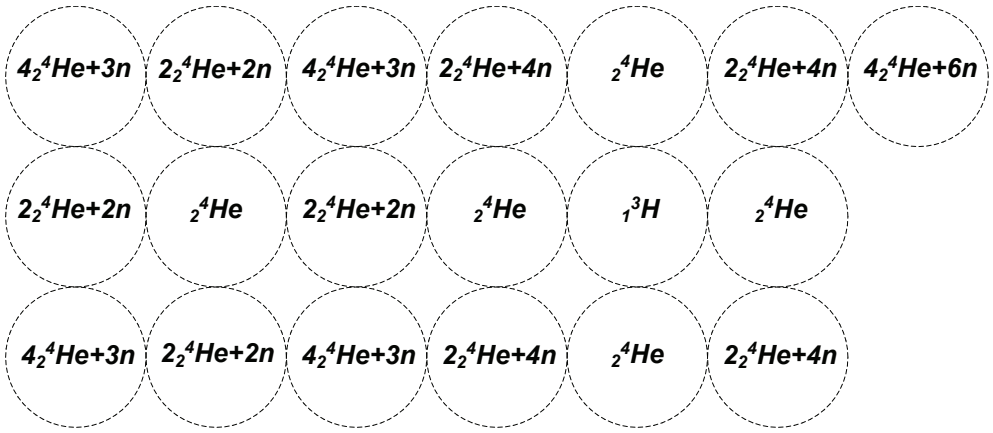

Figure 27. Representation of the bismuth nucleus $^{209}_{83}Bi$, where the addition of four helium nuclei $^{4}_{2}He$ and six bonding neutrons appears adjacent to the corner potential column of the rhenium nucleus $^{187}_{75}Re$

Furthermore, bismuth nucleus $^{209}_{83}Bi$

$$^{209}_{83}Bi =^{187}_{75} Re + 4^{4}_{2}He + 6n \tag{122}$$

is constructed from the addition of four helium nuclei $^{4}_{2}He$ and six bonding neutrons adjacent to the corner potential column of rhenium nucleus $^{187}_{75}Re$.

6.4. Structure model of uranium nucleus $^{235}_{92}U$

The uranium nucleus $^{235}_{92}U$ (Fig. 28)

$$^{235}_{92}U =^{209}_{83} Bi + (^{4}_{2}He +^{3}_{1} H + n) + (2^{4}_{2}He + 2^{3}_{1}H + 4n) \tag{123}$$

is constructed from the addition of one helium nucleus $^{4}_{2}He$, one tritium $1^{3}H$, and one bonding neutron adjacent to the middle potential column of the bismuth nucleus $^{209}_{83}Bi$, while two helium nuclei $^{4}_{2}He$, two tritium nuclei $^{3}_{1}H$, and four bonding neutrons are added at the other corner potential column of the bismuth nucleus.

Therefore, the uranium nucleus $^{235}_{92}U$ is structured from helium nuclei $^{4}_{2}He$ (plus the tritium nuclei $^{3}_{1}H$). The weak link of uranium $^{235}_{92}U$ is the unstable nucleus of the tritium

$^{3}_{1}H$, which is located at its center, where the strong negative electric field of the protons prevails. This critical point becomes an attraction pole of neutrons, i.e., of a thermal neutron and rarely of a fast one, which cleaves it (beta decay β^{-}), incorporating the produced proton into the tritium nucleus $^{3}_{1}H$, turning it into a helium nucleus $^{4}_{2}He$. So, this mechanism acts as a catalyst for the nuclear fission of uranium $^{235}_{92}U$, with the most common products being the barium nucleus $^{141}_{56}Ba$ and the krypton nucleus $^{92}_{36}Kr$, plus three neutrons, as in the nuclear reaction

$$n +^{235}_{92} U \longrightarrow^{141}_{56} Ba +^{92}_{36} Kr + 3n. \tag{124}$$

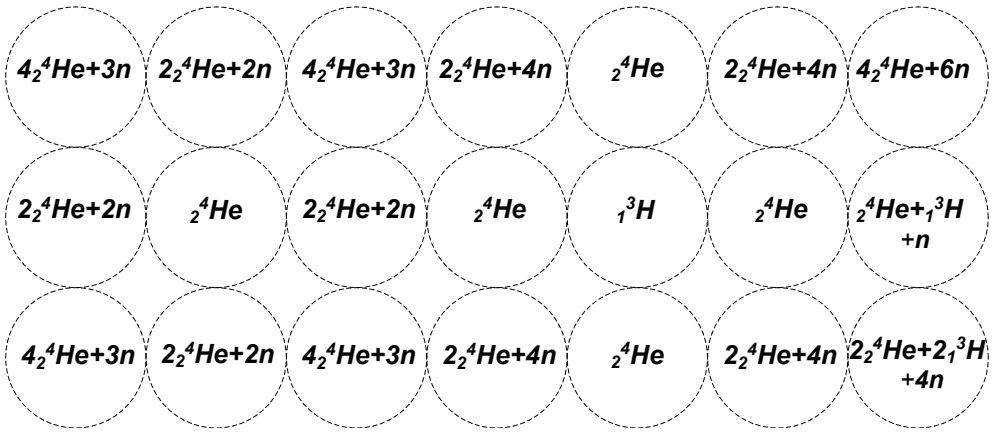

Figure 28. Representation of the uranium nucleus $^{235}_{92}U$, where the addition of one helium nucleus $^{4}_{2}He$, one tritium, and one bonding neutron appears at the middle potential column of the bismuth nucleus $^{209}_{83}Bi$, while the addition of two helium nuclei $^{4}_{2}He$, two tritium nuclei, and four bonding neutrons appears at the other corner potential column of bismuth $^{209}_{83}Bi$

7. References

[1] N.I.Gosdas, *The Unified Theory of Dynamic Space*, Greek Edition (Trohalia, Athens, 1999).

[2] N.I. Gosdas, *The Structure and the Dynamics of Space*, Greek Edition (M.&G. Zorzos, Athens, 2004).

[3] N.I.Gosdas, *The Structure of Nuclei* (chapter 4, pages 69-203), Greek Edition (SALTO, Thessaloniki, 2001).

[4] N.I. Gosdas, *The Structure and Function of the Universe*, Greek Edition (Hellenic Physicists Society, Athens, 2006).

[5] M.Tzoumpas, The Timeless Universe, Greek Edition (Lefkiselida, Athens, 2013.

[6] R.A.Serway, C.J.Moses, C.A.Moyer, *Modern Physics*, English Edition (Saunders College Publishing, 1989).